Acta Crystallographica Section D
Biological Crystallography
ISSN 0907-4449

The structure of dihydrodipicolinate reductase (DapB) from *Mycobacterium tuberculosis* in three crystal forms

Robert Janowski,‡ Georgia Kefala§ and Manfred S. Weiss*

EMBL Hamburg Outstation, c/o DESY, Notkestrasse 85, D-22603 Hamburg, Germany

‡ Present address: IBMB (CSIC), Parc Científic de Barcelona, Baldiri Riexac 10-12, E-08028 Barcelona, Spain.
§ Present address: Salk Institute, 10010 North Torrey Pines Road, La Jolla, CA 92037, USA.

Correspondence e-mail: msweiss@embl-hamburg.de

Received 7 August 2009
Accepted 23 October 2009

PDB References: dihydrodipicolinate reductase, crystal form *A*, 1yl5; crystal form *B*, 1yl6; crystal form *C*, 1yl7.

Dihydrodipicolinate reductase (DHDPR, DapB) is an enzyme that belongs to the L-lysine biosynthetic pathway. DHDPR reduces the α,β-unsaturated cyclic imine 2,3-dihydrodipicolinic acid to yield the compound 2,3,4,5-tetrahydrodipicolinic acid in a pyridine nucleotide-dependent reaction. The substrate of this reaction is the unstable product of the preceding enzyme dihydrodipicolinate synthase (DHDPS, DapA). Here, the structure of apo-DHDPR from *Mycobacterium tuberculosis* is reported in two orthorhombic crystal forms, as well as the structure of DHDPR from *M. tuberculosis* in complex with NADH in a monoclinic crystal form. A comparison of the results with previously solved structures of this enzyme shows that DHDPR undergoes a major conformational change upon binding of its cofactor. This conformational change can be interpreted as one of the low-frequency normal modes of the structure.

1. Introduction

The L-lysine biosynthetic pathway provides both L-lysine for protein synthesis and *meso*-diaminopimelate (*meso*-DAP) for building up the bacterial peptidoglycan cell wall. As shown by Sassetti *et al.* (2003), proper functioning of this pathway is essential for the growth of *Mycobacterium tuberculosis* (Mtb), the causative agent of tuberculosis. The biosynthesis of L-lysine in bacteria as well as in plants starts from the amino acid L-aspartate and can in principle proceed *via* three different routes: the succinylase route (also called the DAP route), the acetylase route and the dehydrogenase route. The most important and most widely realised route of the three is the DAP route, which yields L-lysine from L-aspartate in nine consecutive enzymatically catalysed steps. This route has been postulated as a promising target for antimicrobial intervention strategies (Cox, 1996; Paiva *et al.*, 2001; Hutton *et al.*, 2003). The fact that the pathway is present in microbes and plants but absent in mammals has focused attention on the nine enzymes that belong to the pathway in Mtb: aspartokinase (Ask), aspartate semialdehyde dehydrogenase (Asd), DapA, DapB, DapC, DapD, DapE, DapF and LysA. Inhibition of any one of

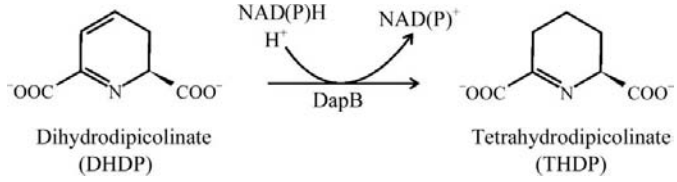

Figure 1
The enzymatic reaction catalysed by DHDPR.

© 2010 International Union of Crystallography
Printed in Singapore – all rights reserved

Table 1
Structurally characterized DHDPRs and DHDPR complexes.

PDB code	Organism	Resolution (Å)	No. of subunits per ASU	Ligands/cofactor	Reference
1dih	*E. coli*	2.20	1	NADPH	Scapin *et al.* (1995)
1dru	*E. coli*	2.20	1	NADH	Reddy *et al.* (1996)
1drv	*E. coli*	2.20	1	Ac-NADH†	Reddy *et al.* (1996)
1drw	*E. coli*	2.20	1	NHDH‡	Reddy *et al.* (1996)
1arz	*E. coli*	2.60	4 (*A*, *B*, *C*, *D*)	NADH/2,6-PDC§¶	Scapin *et al.* (1997)
1p9l	*M. tuberculosis*	2.30	2 (*A*, *B*)	NADH/2,6-PDC	Cirilli *et al.* (2003)
1c3v	*M. tuberculosis*	2.39	2 (*A*, *B*)	NADPH/2,6-PDC	Cirilli *et al.* (2003)
1vm6	*T. maritima*	2.27	4 (*A*, *B*, *C*, *D*)	NADH††	JCSG, unpublished work
1yl5	*M. tuberculosis*	2.30	2 (*A*, *B*)	—	This work
1yl6	*M. tuberculosis*	2.90	2 (*A*, *B*)	—	This work
1yl7	*M. tuberculosis*	2.34	8 (*A*, *B*, *C*, *D*, *E*, *F*, *G*, *H*)	NADH	This work

† 3-Acetyl pyridine adenine dinucleotide. ‡ Nicotinamide hypoxyadenthine dinucleotide. § The cofactor and ligand are only present in chains *B*, *C* and *D*. ¶ Pyridine-2,6-dicarboxylic acid (dipicolinic acid). †† Acetate is present in the active site of chains *A*, *B* and *D*, mimicking the substrate/product/inhibitor.

Table 2
Data-processing, structure-refinement and validation statistics.

Values in parentheses are for the outermost resolution shell.

Crystal form	*A*	*B*	*C*
Space group	$P2_12_12$	$P2_12_12$	*C*2
Unit-cell parameters (Å, °)	$a = 59.26$, $b = 122.00$, $c = 77.93$, $\alpha = \beta = \gamma = 90$	$a = 87.13$, $b = 89.46$, $c = 77.52$, $\alpha = \beta = \gamma = 90$	$a = 238.60$, $b = 67.52$, $c = 154.49$, $\alpha = \gamma = 90$, $\beta = 117.08$
Resolution limits (Å)	30.0–2.30 (2.42–2.30)	30.0–2.90 (3.06–2.90)	30.0–2.34 (2.47–2.34)
Unique reflections	25725	13836	80393
Completeness (%)	99.6	98.9	86.6
$I/\sigma(I)$	17.1	23.9	18.7
$R_{\rm r.i.m.}$ (%)	9.2	6.9	10.0
Data cutoff [$F/\sigma(F)$]	0.0	0.0	0.0
Total No. of reflections	24648	12552	77923
No. of reflections in working set	23592	11315	75495
No. of reflections in test set	1056	1237	2428
R (%)	20.6 (27.9)	19.9 (25.7)	18.1 (21.6)
$R_{\rm free}$ (%)	25.0 (35.1)	25.7 (38.0)	23.8 (29.5)
No. of amino-acid residues	494	490	1952
No. of protein atoms	3648	3622	14495
No. of ligand atoms	—	—	352
No. of ions	2	2	6
No. of solvent atoms	49	2	356
R.m.s.d. bond lengths (Å)	0.013	0.015	0.012
R.m.s.d. bond angles (°)	1.5	1.7	1.4
Ramachandran plot (most favoured)† (%)	90.8	89.6	91.5
PDB code	1yl5	1yl6	1yl7

† The values given refer to the fraction of the amino-acid residues which are part of the refined and deposited model.

these enzymes should affect only the pathogenic organism, with little potential toxicity for the patient (Grandoni *et al.*, 1998).

Dihydrodipicolinate reductase (DHDPR, DapB; EC 1.3.1.26) is one of the enzymes of the L-lysine biosynthetic pathway. It catalyzes the reduction of the α,β-unsaturated cyclic imine 2,3-dihydrodipicolinic acid to 2,3,4,5-tetrahydrodipicolinic acid (Fig. 1). DHDPR can use either NADH or NADPH as cofactor. The enzyme from Mtb (Mtb-DHDPR; Rv2773c) is able to use both NADH and NADPH with nearly equal efficiency, as reported by Cirilli *et al.* (2003), with $K_{\rm m}$ values of 3.2 ± 0.4 and 11.8 ± 1.5 μM, respectively.

To date, DHDPRs from three different bacterial species have been characterized structurally (Table 1). DHDPR from *Escherichia coli* (Ec-DHDPR) has been analyzed as binary complexes with NADPH (PDB entry 1dih; Scapin *et al.*, 1995), NADH, acetyl-NADH and nicotinamide hypoxyadenthine dinucleotide (NHDH) (PDB entries 1dru, 1drv and 1drw, respectively; Reddy *et al.*, 1996). The same enzyme was subsequently crystallized as a ternary complex with NADH and the inhibitor pyridine-2,6-dicarboxylic acid (dipicolinic acid, 2,6-PDC; PDB entry 1arz; Scapin *et al.*, 1997). While only an open conformation of the enzyme was observed for the binary complexes, both an open and a closed conformation were found in the crystal form of the ternary complex. The reason for this is that one of the four subunits in the asymmetric unit of the crystal form was unliganded (chain *A*) and adopted an open conformation, even though both cofactor and inhibitor were bound in the other three (chains *B*, *C* and *D*), leading to a closed conformation of the enzyme. An open and a closed conformation have been also observed for DHDPR from *Thermotoga maritima* (Tm-DHDPR), which was crystallized in the presence of NADH (PDB entry 1vm6, Joint Center for Structural Genomics, unpublished data). The asymmetric unit of the crystal contains four subunits, which form the physiologically relevant tetramer. One subunit (chain *C*) contains only NADH and adopts an open conformation, while in the other three subunits (chains *A*, *B* and *D*) an acetate ion was observed in the active site which binds in the same position as one of the carboxylate groups of 2,6-PDC in Ec-DHDPR. These three chains adopt a conformation between the open and the closed states. For Mtb-DHDPR only the structures of the ternary complexes with NADH and 2,6-PDC and with NADPH and 2,6-PDC are known (Cirilli *et al.*, 2003). In both cases the enzyme only occurs in the closed conformation.

Here, we report for the first time the structure of Mtb-DHDPR in its apo form and as a binary complex with its cofactor NADH, thus completing the picture for the Mtb enzyme. A detailed comparison with all other known DHDPRs is presented, which reveals some details of the domain motions that occur as a result of substrate and/or cofactor binding.

2. Materials and methods

2.1. Cloning, expression, purification and crystallization

The cloning, expression, purification and crystallization of DHDPR from *M. tuberculosis* as well as the results of the diffraction experiments have been described previously (Kefala *et al.*, 2005). Briefly, three crystal forms were obtained which were suitable for structure analysis. These forms have been labelled forms *A*, *B* and *C*. Forms *A* and *B* (both of which belong to space group $P2_12_12$) were obtained for the apo-enzyme, while form *C* (belonging to space group *C*2) was obtained for enzyme crystallized in the presence of its cofactor NADH. Diffraction data have been collected to resolutions of 2.30, 2.90 and 2.34 Å for forms *A*, *B* and *C*, respectively (see Table 2 and Table 1 of Kefala *et al.*, 2005).

2.2. Structure determination and refinement

The structures of all three polymorphic forms were determined by molecular replacement using the program *MOLREP* (Vagin & Teplyakov, 1997; Collaborative Compu-

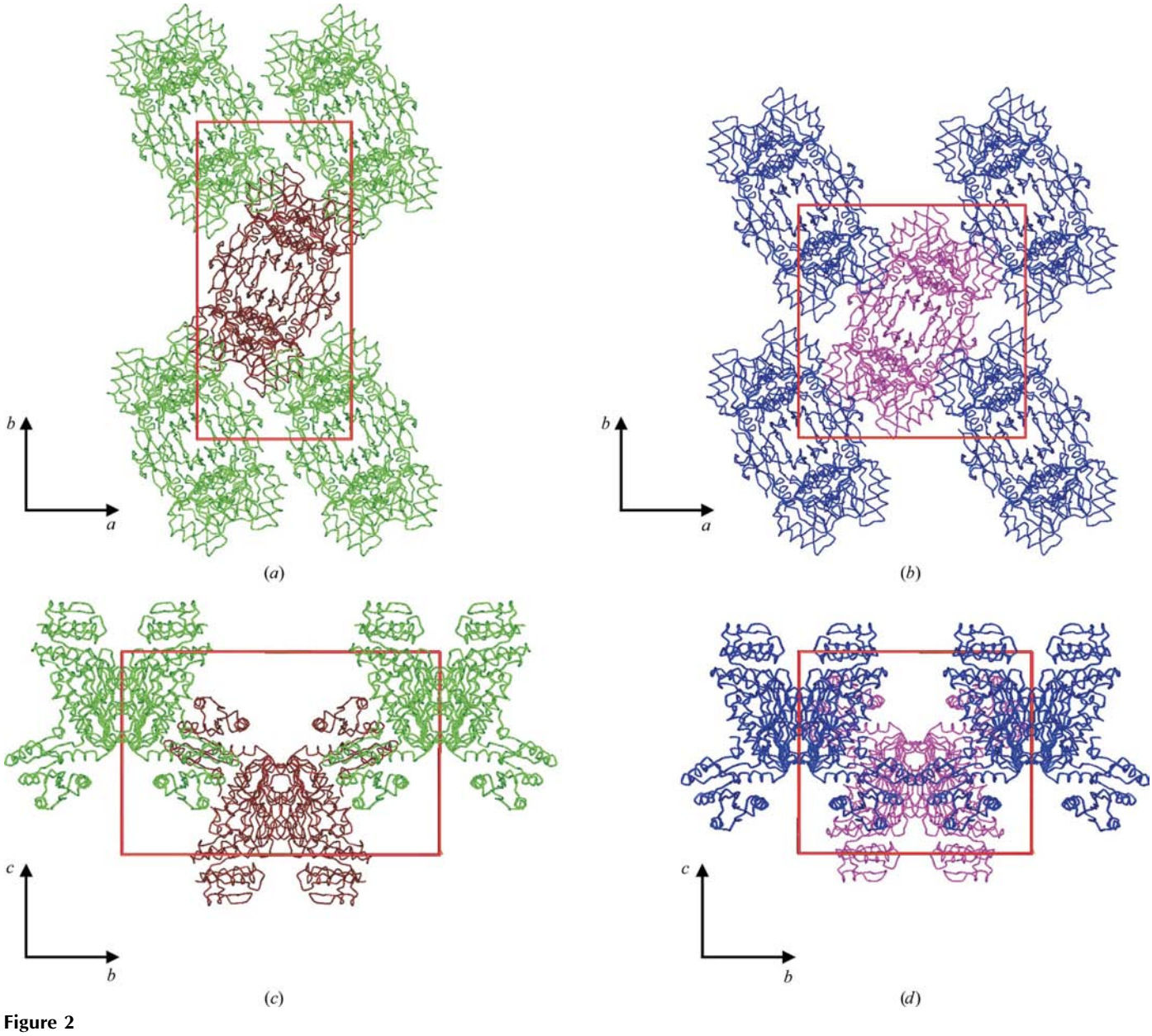

Figure 2
Crystal packing of the Mtb-DHDPR tetramers in crystal forms *A* and *B*. Projections are shown along the *c* axis for crystal forms *A* (*a*) and *B* (*b*) and along the *a* axis for crystal forms *A* (*c*) and *B* (*d*). The figure was prepared using the program *ViewerLite* v.4.2 (Accelrys Inc.; http://www.accelrys.com).

Table 3
Superposition of the 12 independent monomers of the three crystal forms of Mtb-DHDPR calculated using *ALIGN*.

Each comparison is characterized by an r.m.s. deviation (Å) between the superimposed C^{α} atoms and by the number of superimposed atom pairs (in parentheses). R.m.s. deviations of greater than 2 Å are highlighted in bold.

	1yl5_*A*	1yl5_*B*	1yl6_*A*	1yl6_*B*	1yl7_*A*	1yl7_*B*	1yl7_*C*	1yl7_*D*	1yl7_*E*	1yl7_*F*	1yl7_*G*
1yl5_*A*	0.0										
1yl5_*B*	0.43 (243)	0.0									
1yl6_*A*	0.39 (241)	0.49 (240)	0.0								
1yl6_*B*	0.41 (242)	0.47 (240)	0.12† (222)	0.0							
1yl7_*A*	1.13 (244)	1.21 (244)	1.32 (245)	1.25 (244)	0.0						
1yl7_*B*	0.85 (239)	1.08 (240)	1.02 (249)	1.02 (240)	0.81 (244)	0.0					
1yl7_*C*	1.31 (241)	1.41 (243)	1.44 (242)	1.44 (244)	1.06 (244)	0.85 (243)	0.0				
1yl7_*D*	1.31 (243)	1.38 (243)	1.45 (243)	1.38 (242)	0.54 (244)	1.15 (244)	1.53 (244)	0.0			
1yl7_*E*	**2.25 (234)**	**2.36 (230)**	**2.29 (233)**	**2.31 (234)**	**2.15 (231)**	**2.18 (231)**	**2.35 (219)**	**2.01 (233)**	0.0		
1yl7_*F*	0.63 (242)	0.91 (242)	0.70 (242)	0.76 (242)	1.24 (241)	0.72 (243)	1.33 (244)	1.47 (243)	**2.11 (233)**	0.0	
1yl7_*G*	1.08 (242)	1.25 (242)	1.25 (242)	1.22 (242)	0.45 (244)	0.65 (244)	1.14 (244)	0.65 (244)	**2.03 (233)**	1.09 (244)	0.0
1yl7_*H*	1.16 (242)	1.38 (243)	1.32 (242)	1.33 (243)	0.91 (244)	0.55 (242)	0.77 (243)	1.30 (244)	**2.23 (230)**	1.01 (243)	0.73 (243)

† Since NCS restraints were used in the refinement, this r.m.s.d. value is artificially low.

tational Project, Number 4, 1994). The search model used was the 2.3 Å resolution structure of Mtb-DHDPR in complex with NADH and dipicolinic acid (PDB code 1p9l; Cirilli *et al.*, 2003). All heteroatoms were removed from the search model and only one subunit was used for the calculations. Owing to problems with refinement of the solutions in all three cases (see discussion below), the molecular-replacement search was repeated with the search model divided into two separate domains. Initially, *MOLREP* was run with the tetramerization domain only (the C-terminal domain). Subsequently, it was run with the N-terminal, substrate and inhibitor binding domain. In the case of crystal forms *A* and *B* two molecules were found to occupy the asymmetric unit. They form homodimers, which assemble into homotetramers by means of the crystallographic twofold symmetry axis along *c*. Crystal form *C* contains eight monomers in the asymmetric unit, which assemble into two complete and independent homotetramers. Structure refinement was performed using *REFMAC*5 (Murshudov *et al.*, 1997), making use of the maximum-likelihood target function and including TLS parameters (Winn *et al.*, 2001). Noncrystallographic symmetry (NCS) restraints were included in refinement of the form *B* structure owing to the lower number of observed reflections compared with forms *A* and *C*. After cycling between manually rebuilding the model in *O* (Jones *et al.*, 1991) and further refinement, the final refined models were characterized by *R* and $R_{\rm free}$ values of 20.6% and 25.0% (crystal form *A*), 19.9% and 25.7% (crystal form *B*) and 18.1% and 23.8% (crystal form *C*), respectively. The numerical details concerning the refinement of all three structures are presented in Table 2. The refined structures and the corresponding structure-factor amplitudes have been deposited in the PDB with accession codes 1yl5, 1yl6 and 1yl7 for crystal forms *A*, *B* and *C*, respectively.

2.3. Structure validation and analysis

Stereochemical analysis of the final models was performed using the program *PROCHECK* (Laskowski *et al.*, 1993). The *DynDom* server (Hayward & Berendsen, 1998) was used to analyze the domain motion of DHDPR. The Error-inclusive Structure Comparison and Evaluation Tool (*ESCET* v.0.6b; Schneider, 2002) was also applied for the same purpose.

2.4. Identification of DHDPR homologues and structural superpositions

Similar and homologous structures were identified by secondary-structure matching using the *SSM* server (http://www.ebi.ac.uk/msd-srv/ssm; Krissinel & Henrick, 2004) using subunit *A* of PDB entry 1yl5 as the search model. Structure comparisons and superpositions were carried out using the programs *ALIGN* (Cohen, 1997) and *LSQKAB* (Collaborative Computational Project, Number 4, 1994; Kabsch, 1976).

2.5. Normal-mode analysis

In order to investigate the flexibility and conformational changes, the low-frequency normal modes of DHDPR were computed using *The Elastic Network Model* (*elNémo*) server (Suhre & Sanejouand, 2004). Chains *A* (open form) and *E* (closed form) from crystal form *C* (PDB entry 1yl7) of Mtb-DHDPR were used for the calculations. For each chain, five low-frequency normal modes were analysed. Each normal mode is illustrated by a set of 11 coordinate sets, with the original submitted coordinates constituting the central set. On each side of the central coordinate set five conformations are given as intermediate structures towards the most extreme conformers. The similarity between the predicted conformers and the observed structures was assessed by least-squares superposition using the program *LSQKAB* (Collaborative Computational Project, Number 4, 1994; Kabsch, 1976). In this case, the whole molecules were analysed. For the purpose of illustrating how the predicted conformers fit to the observed crystal structures, the normal-mode conformers and the observed crystal structures were superimposed based on their N-terminal domains only in order to enhance the effect of the movement of the tetramerization domain.

3. Results and discussion

3.1. The refined structures

Analysis of the stereochemical quality of the refined models revealed that 90.8, 89.6 and 91.5% of all residues in crystal forms *A*, *B* and *C*, respectively, fall into the core region of the Ramachandran plot; no residues were found with generously allowed or unfavourable backbone dihedral angles. For crystal form *A* all residues of both independent molecules in the asymmetric unit except for the C-terminal His245 were clearly visible in the ($2F_{obs} - F_{calc}$, α_{calc}) electron-density map contoured at 1σ. In addition, two extra residues, Ala and Met, were visible at the N-terminus and are cloning artifacts (Kefala *et al.*, 2005). For crystal forms *B* and *C*, which were obtained from DHDPR construct No. 1 (Kefala *et al.*, 2005), the first residue (Met1) was only observed to be ordered in the two molecules of crystal form *B*. His245 was poorly ordered in most of the chains of crystal forms *B* and *C*. Consequently, only some atoms of this residue were included in the model. The amino acids following His245, containing the thrombin cleavage site and the His_6 tag (which is still present in the expressed protein; Kefala *et al.*, 2005), were found to be disordered in all molecules of crystal forms *B* and *C*. The good quality of the electron-density maps allowed the inclusion of water molecules as well as of magnesium ions (see Table 2 for details). Based on the ($F_{obs} - F_{calc}$, α_{calc}) electron-density map, NADH molecules were placed in the cofactor-binding site of all eight independent molecules of the monoclinic form *C* crystals. The root-mean-square deviation (r.m.s.d.) values between all pairs of refined Mtb-DHDPR molecules ranged from 0.39 to 2.36 Å^2 (Table 3). The conclusions arising from these r.m.s.d. values will be discussed separately in §3.5. The sequence of the *dapB* gene encoding DHDPR from *M. tuberculosis* strains H37Rv and CDC1551 indicates the presence of an alanine residue at position 14 (Cole *et al.*, 1998), while the sequence of this gene published by Pavelka *et al.* (1997), as well as the crystal structures of this protein reported by Cirilli *et al.* (2003), contained a threonine residue in this position. In our studies, position 14 of the amino-acid sequence was occupied by Ala. This has been confirmed by sequencing of DHDPR constructs Nos. 1 and 2 and is supported by clear electron density for this region in all 12 refined amino-acid chains of Mtb-DHDPR presented in this work.

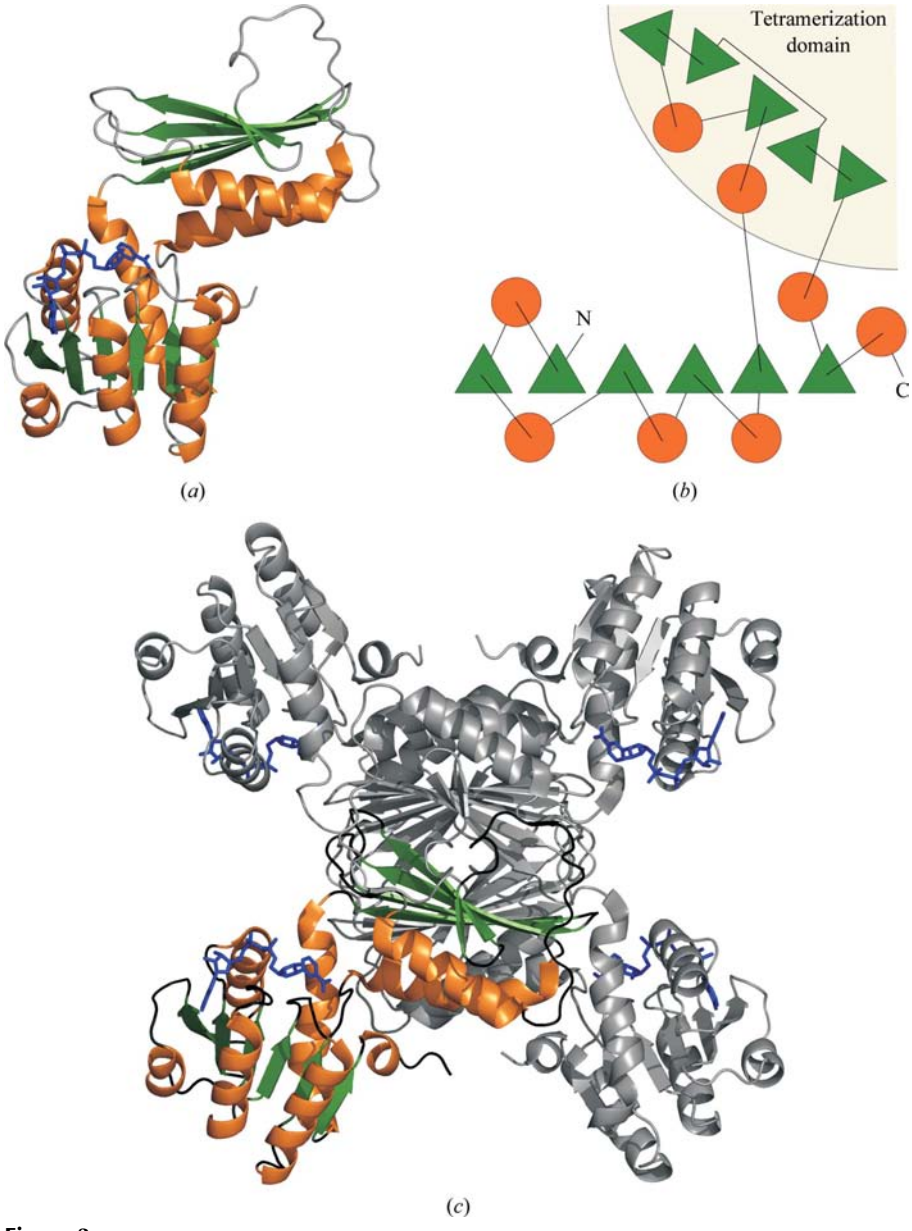

Figure 3
The structure of Mtb-DHDPR in the open conformation (shown are subunits *A*, *B*, *C* and *D* from the monoclinic crystal form *C*). (*a*) depicts a ribbon representation of one subunit of Mtb-DHDPR, (*b*) shows the corresponding topology diagram and (*c*) shows the whole biologically relevant tetramer assembly with one monomer coloured and the other three chains shown in grey. α-Helices are shown in orange, β-strands in green and the NADH cofactor in navy blue.

3.2. Crystal packing

Since crystal forms *A* and *B* exhibit the same orthorhombic symmetry, the same number of molecules in the asymmetric unit, similar unit-cell volumes (563 412 and 604 241 Å^3 for forms *A* and *B*, respectively) and the same length of the *c* axis (see Table 2), it seems interesting and informative to compare the packing of the DHDPR tetramers in these forms in more detail. The orientation of the tetramers with

respect to the axes in both unit cells is nearly the same (Fig. 2). The only difference between the two forms is the rotation of a tetramer by approximately 3.5° around the *c* axis. This rotation is accompanied by a translation of the tetramers in the unit cell along the unit-cell axes. Both crystal forms contain two complete tetramers in the unit cell, the centres of which are located at the edges of the unit cell ($a = b = 0$) and in the centre ($a = b = 1/2$). This becomes apparent when looking along the *c* axis. (Note: the *c* axis is the one along which the crystallographic twofold axis is located. The tetramer is formed about this axis from the dimer present in the asymmetric unit.) The distances between the centres of the adjacent edge tetramers are equal to the unit-cell parameters *a* and *b*, while the distance between an edge tetramer and the central tetramer in *a* and *b* is the half-diagonal. Along the *c* direction, the distances between the central and the edge tetramers are 36.8 Å in form *A* and 20.3 Å in form *B*. This means that the crystal packing in the *c* direction, as well as in the *b* direction, is more compact in crystal form *B*, while in crystal form *A* the packing is more compact in the *a* direction. As a result, the crystal contacts differ in the two polymorphic forms. In crystal form *A* the edge tetramers (depicted in green in Figs. 2*a* and 2*c*) only interact with the central tetramers (depicted in brown in Figs. 2*a* and 2*c*), but not with other edge tetramers. This is in contrast to the situation in crystal form *B*, in which the edge tetramers (depicted in blue in Figs. 2*b* and 2*d*) interact with the central tetramers (depicted in magenta in Fig. 2*b*) as well as with neighbouring edge tetramers *via* a few contacts between α-helices located around the twofold axis along the *c* direction. Various projections of the crystal packing of Mtb-DHDPR tetramers in crystal forms *A* and *B* are illustrated in Fig. 2.

Table 4
Comparison of the different DHDPR structures with the structures of Mtb-DHDPR subunits *A* (1yl7_*A*) and *E* (1yl7_*E*) from crystal form *C*.

Values in parentheses correspond to the number of superimposed C^{α} atoms.

PDB code and chain ID	Organism	Cofactor/ligand	R.m.s.d. to 1yl7_*A* 'open'	R.m.s.d. to 1yl7_*E* 'closed'	Conformation
1yl5_*A*	*M. tuberculosis*	—	1.12 (243)	2.25 (236)	Open
1yl5_*B*		—	1.20 (243)	2.37 (233)	Open
1yl6_*A*	*M. tuberculosis*	—	1.31 (244)	2.29 (235)	Open
1yl6_*B*		—	1.25 (244)	2.30 (236)	Open
1yl7_*A*	*M. tuberculosis*	NADH	—	2.19 (234)	Open
1yl7_*E*			2.19 (234)	—	Closed
1p9l_*A*	*M. tuberculosis*	NADH/2,6-PDC†	2.57 (228)	0.89 (242)	Closed
1p9l_*B*		NADH/2,6-PDC	2.51 (230)	0.90 (243)	Closed
1c3v_*A*	*M. tuberculosis*	NADPH/2,6-PDC	2.64 (231)	0.86 (243)	Closed
1c3v_*B*		NADPH/2,6-PDC	2.58 (231)	0.85 (244)	Closed
1arz_*A*	*E. coli*	—	1.67 (209)	2.32 (201)	Open
1arz_*B*		NADH/2,6-PDC	2.90 (210)	1.69 (215)	Closed
1arz_*C*		NADH/2,6-PDC	2.92 (209)	1.71 (215)	Closed
1arz_*D*		NADH/2,6-PDC	2.75 (203)	1.71 (215)	Closed
1dih	*E. coli*	NADPH	1.91 (211)	2.77 (206)	Open
1dru	*E. coli*	NADH	1.68 (210)	1.91 (200)	Open
1drv	*E. coli*	Ac-NADH‡	1.61 (209)	1.92 (199)	Open
1drw	*E. coli*	NHDH§	1.81 (207)	2.84 (209)	Open
1vm6_*A*	*T. maritima*	NADH/acetate	2.74 (199)	1.86 (203)	Closed
1vm6_*B*		NADH/acetate	2.87 (201)	1.95 (201)	Closed
1vm6_*C*		NADH	1.65 (199)	2.70 (197)	Open
1vm6_*D*		NADH/acetate	3.03 (203)	1.93 (201)	Closed

† Pyridine-2,6-dicarboxylic acid (dipicolinic acid). ‡ 3-Acetyl pyridine adenine dinucleotide. § Nicotinamide hypoxyadenthine dinucleotide.

3.3. The overall structure

The overall fold of DHDPR has been described previously for the enzymes from *E. coli* (Scapin *et al.*, 1995, 1997; Reddy *et al.*, 1996), from *M. tuberculosis* (Cirilli *et al.*, 2003) and from *T. maritima* (Joint Center of Structural Genomics, unpublished work). In brief, the three-dimensional structure of DHDPR consists of two domains: an N-terminal domain responsible for cofactor binding and a C-terminal domain that is mainly responsible for tetramerization of the enzyme (Fig. 3*a*). The C-terminal domain also harbours the substrate-binding site. The N-terminal domain consists of amino-acid residues Met1–Ala106 and Ser216–His245 and is built up of a six-stranded β-sheet flanked by four α-helices. It is similar but not identical to the typical nucleotide-binding fold defined by Rossmann *et al.* (1975). The tetramerization or substrate/inhibitor-binding domain consists of the 109 amino-acid residue sequence segment Ile107–Thr215. It folds into a five-stranded β-sheet and two α-helices, which assemble into an αβ-sandwich (Fig. 3*b*). Formation of the homotetramer occurs exclusively *via* the C-terminal domain. Upon tetramerization, a 16-stranded β-barrel surrounded by eight α-helices is formed (Fig. 3*c*). The N-terminal domains do not interact with each other at all in the tetramer. The two domains are rather flexibly connected to each other by two loops, leaving room for a large motion of one domain relative to the other. It is important to mention that the quality of the ($2F_{obs} - F_{calc}$, α_{calc}) map is always lower for the N-terminal domain compared with that for the inner more rigid tetramerization domain. This observation fits nicely with the fact that the average value of the atomic displacement parameters (ADPs) is significantly higher for the N-terminal domain than for the C-terminal tetramerization domain, especially for the eight subunits in crystal form *C* (47 *versus* 33 $Å^2$).

3.4. Cofactor binding

Strong positive difference electron density was observed in the dinucleotide-binding site of all eight molecules in the

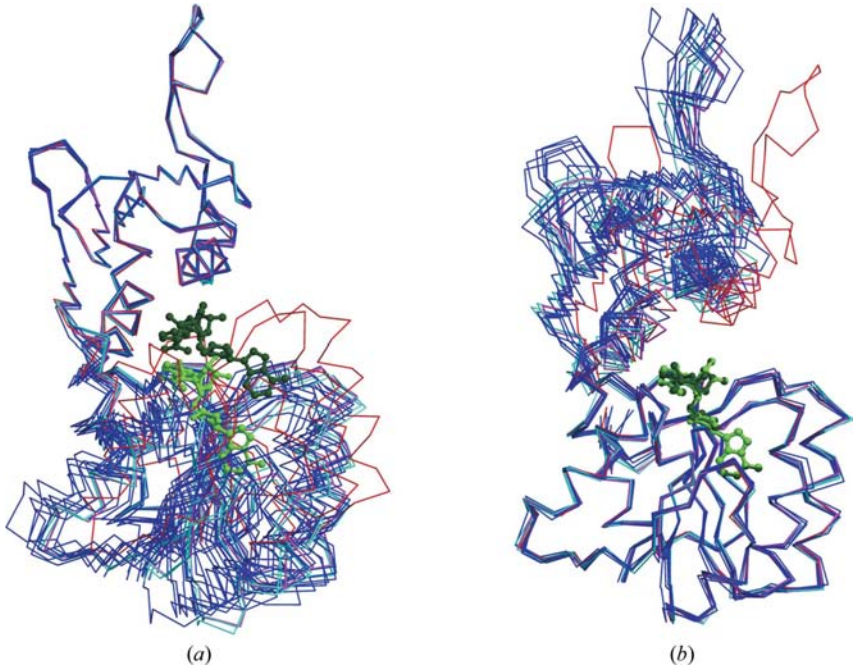

Figure 4
The different conformations of Mtb-DHDPR as observed in the three crystal forms *A*, *B* and *C*. The superposition was prepared using the C^{α} atoms from one domain only in order to emphasize the differences between the molecules in the other domain. (*a*) shows the superposition based on the C-terminal or tetramerization domain, while (*b*) shows the superposition based on the N-terminal domain. The figure also highlights the binding site of the cofactor NADH. The different DHDPR molecules are labelled as follows. Chain *E* from the monoclinic crystal form *C* is shown in red, while the other seven chains from this form are shown in blue. Cyan represents both chains of crystal form *A* and magenta corresponds to the two chains observed in crystal form *B*. NADH molecules are shown in light and dark green. The NADH structures were taken from subunits *A* and *E* of the monoclinic crystal form *C*, respectively. The figure was prepared using the programs *MOLSCRIPT* (Kraulis, 1991) and *Raster3D* (Merritt & Bacon, 1997).

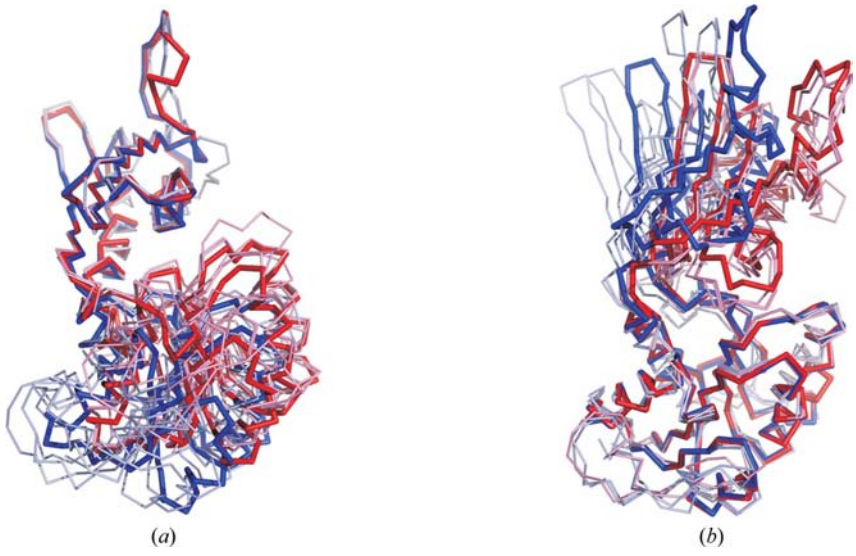

Figure 5
Comparison of the open and closed forms of DHDPR. Mtb-DHDPR chains *A* (open form) and *E* (closed form) from crystal form *C* (shown in dark blue and red, respectively) were superimposed with selected previously published DHDPR structures. The open conformations observed in Ec-DHDPR (PDB entry 1dih, Scapin *et al.*, 1995; chain *A* of PDB entry 1arz, Scapin *et al.*, 1997) are shown in light blue, while the closed conformations observed in Mtb-DHDPR (chain *A* of PDB entries 1p9l and 1c3v, Cirilli *et al.*, 2003) are depicted in light red. The superposition was prepared in the same way as that presented in Fig. 4. (*a*) shows the superposition based on the C-terminal or tetramerization domain, while (*b*) shows the superposition based on the N-terminal domain. This figure was prepared using *PyMOL* (DeLano, 2002).

asymmetric unit of the monoclinic crystal form *C*. This density was interpreted as NADH, since NADH had also been used in crystallization (Kefala *et al.*, 2005). NADH binds in the same manner as previously observed for Mtb-DHDPR (Cirilli *et al.*, 2003). The dinucleotide lies across the C-terminal end of the central β-sheet of the N-terminal domain in an extended conformation (Fig. 3*a*). It forms an extended network of hydrogen bonds with amino-acid residues Gly7, Gly10, Lys11, Val12, Asp33, Gly75, Thr77, Ala102 and Phe105.

3.5. Structure comparisons

A comparison of the independent molecules of the Mtb-DHDPR apoenzyme and the Mtb-DHDPR–NADH complex shows no significant differences, with the exception of chain *E* from crystal form *C*. The corresponding r.m.s.d. values between the superimposed C^{α} atoms range from 0.39 to 1.53 Å (Table 3). The largest difference occurs between chains *C* and *D* from the monoclinic crystal form *C*. However, the r.m.s.d. values increase and exceed 2 Å when chain *E* from the monoclinic form is taken into account in the comparison. Fig. 4 shows a superposition of the 12 independent Mtb-DHDPR structures reported here. The superposition was prepared using the C^{α} atoms from one domain only in order to highlight the differences in the other domain. This was performed separately for the rigid C-terminal tetramerization and substrate/inhibitor-binding domain (Fig. 4*a*) and the more flexible N-terminal cofactor-binding domain (Fig. 4*b*). As is evident, especially in Fig. 4(*b*), subunit *E* from the monoclinic crystal form *C* possesses a different relative orientation of its two domains, which explains the rather high r.m.s.d. value to the other subunits. All the other non-*E*-like subunits exhibit a similar conformation. Consequently, for all further structure comparisons subunit *A* from crystal form *C* will be chosen as a representative of this group. An important question to answer is whether the observed closed conformation of Mtb-DHDPR in complex with NADH as

Table 5
Comparison of the main-chain dihedral angles (φ, ψ) for the amino acids of the two hinge regions in the various DHDPR structures.

(*a*) *M. tuberculosis*.

	Asn104	Phe105	Ala106	Asp213	Arg214	Thr215
1yl7_*A*_open	−152/104	−88/−1	−78/107	−151/160	−73/−14	−66/−20
1yl7_*B*_open	−156/119	−100/−3	−76/110	−170/−171	−68/−8	−83/4
1yl7_*C*_open	−150/109	−90/12	−90/112	−178/178	−73/12	−93/−2
1yl7_*D*_open	−141/112	−93/2	−83/111	−163/157	−74/−12	−66/−19
1yl7_*E*_closed	−154/121	−88/−5	−80/123	−153/146	−66/−14	−66/−20
1yl7_*F*_open	−169/126	−115/1	−77/115	−156/157	−46/−30	−79/17
1yl7_*G*_open	−139/122	−99/−1	−81/115	−164/155	−77/−6	−70/−18
1yl7_*H*_open	−159/115	−97/−1	−80/112	−156/157	−58/−12	−82/−3
1yl5_*A*_open	−163/123	−111/−3	−73/123	−113/164	−83/−13	−109/31
1yl5_*B*_open	−153/120	−110/−2	−72/108	−137/149	−70/−12	−112/24
1yl6_*A*_open	−162/124	−108/−7	−69/112	−131/144	−50/−40	−91/16
1yl6_*A*_open	−159/122	−110/−2	−73/109	−130/152	−62/−28	−90/9
1p9l_*A*_closed	−164/136	−104/−5	−74/135	−151/150	−69/−11	−66/−22
1p9l_*B*_closed	−162/136	−103/−5	−74/137	−149/149	−71/−10	−66/−23
1c3v_*A*_closed	−160/130	−98/−3	−75/130	−139/145	−67/−12	−69/−17
1c3v_*B*_closed	−160/130	−98/−3	−75/130	−139/145	−68/−12	−69/−17

(*b*) *E. coli*.

	Asn128	Phe129	Ser130	Ser239	Arg240	Met241
1arz_*A*_open	−158/105	−82/26	−91/133	−145/164	−78/10	−68/−40
1arz_*B*_closed	−152/134	−108/30	−106/162	−152/139	−60/−15	−59/−30
1arz_*C*_closed	−154/136	−110/29	−104/164	−150/142	−60/−16	−58/−31
1arz_*D*_closed	−153/136	−109/29	−105/163	−149/139	−60/−17	−56/−32
1dih_open	−153/110	−91/4	−69/128	−157/177	−87/6	−59/−25
1dru_open	−138/128	−112/15	−84/122	−160/160	−63/−6	−62/−30
1drv_open	−145/120	−97/13	−86/125	−157/152	−64/−8	−69/−24
1drw_open	−153/113	−94/12	−72/131	−162/179	−86/−5	−55/−34

(*c*) *T. maritima*.

	Asn97	Phe98	Ser99	Ser183	Arg184	Thr185
1vm6_*A*_closed	−152/123	−102/29	−98/152	−141/168	−65/−20	−55/−35
1vm6_*B*_closed	−155/120	−99/30	−97/158	−150/169	−61/−23	−57/−31
1vm6_*C*_open	−151/114	−99/17	−65/122	174/179	−59/−22	−58/−29
1vm6_*D*_closed	−155/121	−103/22	−90/159	−140/169	−63/−21	−58/−33

observed in subunit *E* of crystal form *C* is a crystallization artifact, since an open conformation of this subunit would not fit into the crystal packing. An analysis of the crystal packing shows that subunit *G* from the adjacent tetramer is indeed situated close to the N-terminal domain of subunit *E*. Replacement of subunit *E* in the observed closed conformation by another subunit in the open-conformation would therefore result in severely overlapping side chains and clashes in the crystal lattice. It could therefore be argued that the crystal packing enforces the observed conformational rearrangement of subunit *E*. In contrast, however, it is also possible that the predisposition of the Mtb-DHDPR–NADH complex to assume this particular closed conformation even in solution may make the observed crystal packing possible in the first place.

A comparison of subunits *A* and *E* from the monoclinic crystal form *C* with the conformations observed for Mtb-DHDPR in PDB entries 1p9l and 1c3v (Cirilli *et al.*, 2003), as well as with those of Ec-DHDPR in PDB entries 1arz and 1dih (Scapin *et al.*, 1995, 1997; Reddy *et al.*, 1996), produces more evidence for a dramatic conformational rearrangement along the reaction coordinate (Fig. 5). The numbers presented in Table 4 clearly show that depending on the presence or absence of the cofactor/substrate/inhibitor DHDPR can adopt either an open or a closed conformation. This observation is independent of the source of DHDPR; it can be observed in the enzymes from both *M. tuberculosis* and *E. coli*. A somewhat surprising observation, however, is the fact that Mtb-DHDPR can assume the closed conformation as a binary complex with just its cofactor bound. Previously, the closed conformation could only be observed in the ternary complex. Based on this observation, one may speculate whether the binary complex constitutes a defined intermediate state along the reaction coordinate. The course of the reaction may thus be described as follows. At first, the apoenzyme occurs exclusively in the open conformation. The cofactor (NADH or NADPH) then binds and the enzyme moves into an equilibrium between the open and closed state. Finally, the substrate binds, shifting the equilibrium to the closed state and thus bringing the enzyme into an enzymatically competent conformation. This description fits nicely with the ordered reaction mechanism with reduced nucleotide binding preceding substrate binding that has been observed for Ec-DHDPR (Reddy *et al.*, 1995) as well as with some experimental evidence for a conformational change occurring in Ec-DHDPR in solution upon binding of NADH and PDC (Wang & Tang, 1997). In retrospect, the presence of two conformational states of DHDPR explains the problems in structure solution by molecular replacement and the refinement of the initial solution obtained from *MOLREP*. The model used to solve the structure was based on PDB entry 1p9l (Cirilli *et al.*, 2003), in which all subunits occur in the closed conformation. In contrast to this, 11 of the 12 subunits found in the three crystal forms of Mtb-DHDPR occur in the open form.

3.6. Domain division and analysis of flexibility

As mentioned above, the three-dimensional structure of Mtb-DHDPR can be divided into two structural domains: the N-terminal dinucleotide-binding domain and the C-terminal substrate/inhibitor-binding domain. Although the C-terminal

domain is the smaller of the two, it is more rigid than the N-terminal domain. An analysis of the average main-chain atomic displacement parameters (Collaborative Computational Project, Number 4, 1994) yielded values of 33 and 47 Å^2 for the C-terminal and N-terminal domains in the monoclinic crystal form *C*, respectively. The reason for this discrepancy is probably the fact that the C-terminal domains of the four subunits of a homotetramer form a rather rigid core. In the orthorhombic crystal forms *A* and *B* this discrepancy is not as pronounced, which may be a consequence of a more extensive involvement of the N-terminal domain in crystal contacts. The definition of the actual boundaries between the structural domains often bears an element of ambiguity. If the structures of subunits *A* and *E* of crystal form *C* are compared using the *DynDom* server (Hayward & Berendsen, 1998) the N-terminal dinucleotide-binding domain is delineated by residues Met1–Ile107 and Asp213–His245, while the remaining residues, Gly108–Leu212, belong to the C-terminal tetramerization domain. These results may differ slightly depending on which pair of subunits is analysed in this way. An analysis of all available Mtb-DHDPR subunits using *ESCET* (Schneider, 2002) identifies the domain border as being between residues Phe105 and Ala106, and between Phe217 and Val218. The ambiguity may be a consequence of the presence of linkers which serve as hinges between the two domains. According to Cirilli *et al.* (2003) the hinge regions of Mtb-DHDPR are composed of the residue segments Pro103–Ala106 and Leu212–Thr215, whereas *DynDom* analysis defines the hinge fragments mainly responsible for the domain movement as Ala106–Ser112 and Asp210–Arg214. An analysis of the main-chain torsion angles of several amino acids in the hinge regions revealed that significant movement of the whole cofactor-binding domain relative to the substrate/inhibitor-binding domain can result from a number of small changes (Table 5, Fig. 6). The whole domain movement can also be described by a single swing angle between the two domains. A more quantitative measure of this swing angle can be obtained by first superposing one domain of one subunit onto the same domain of the second subunit and then calculating the rotation angle that would bring the remaining domains into superposition. If the tetramerization domain of the subunit *A* from the monoclinic crystal form *C* is superimposed onto the respective domain of subunit *A* of PDB entry 1p9l (Cirilli *et al.*, 2003), a swing angle of 25.8° would be required to rotate the N-terminal domains onto each other (Fig. 7). If the same is performed with subunit *E* and PDB entry 1p9l, a swing angle of 7.6° results. When subunits *A* and *E* are compared with each other the swing angle is 22.4°. These

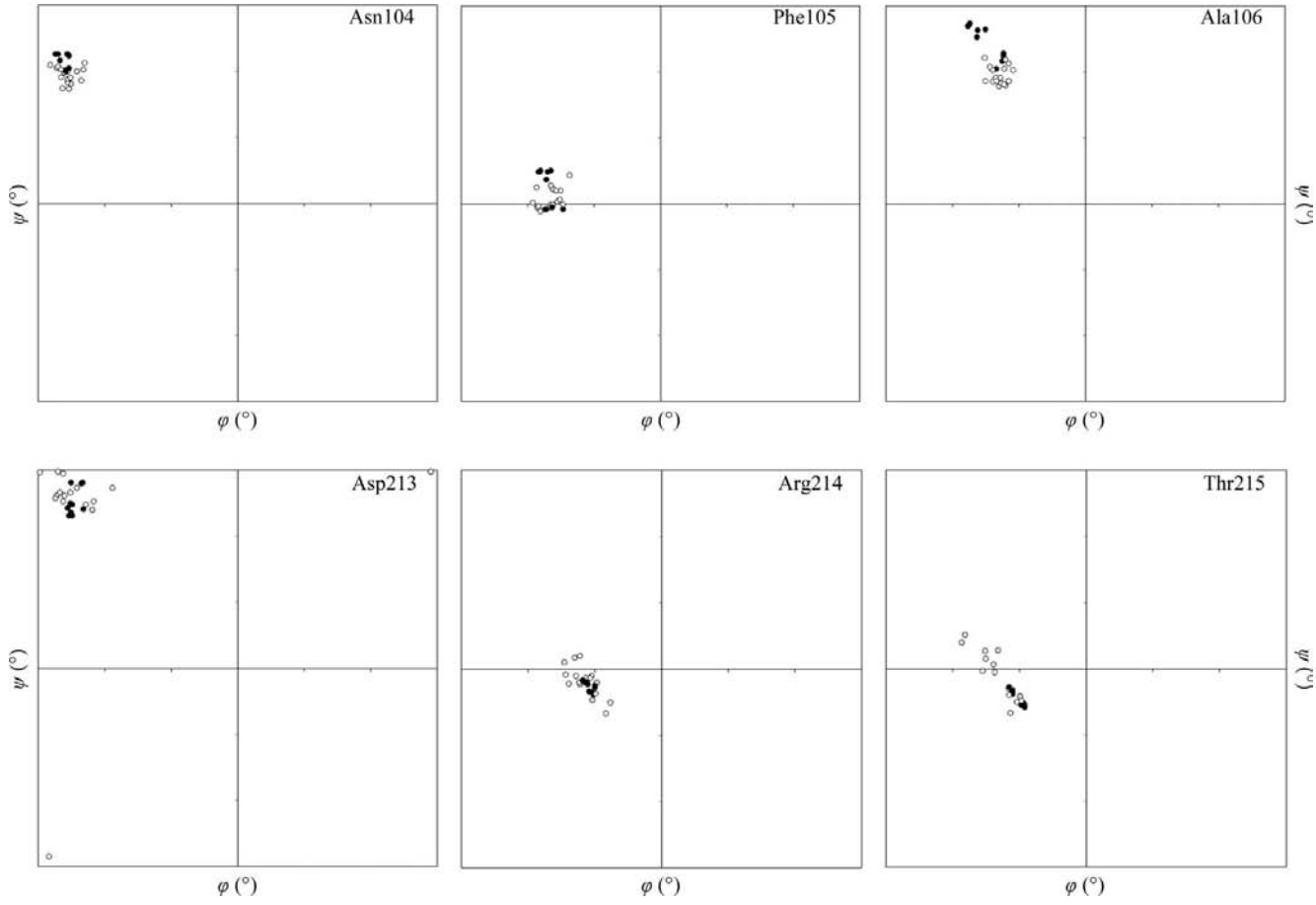

Figure 6
Main-chain dihedral angle (φ, ψ) changes of the amino acids in the two hinge regions identified in DHDPR. The amino-acid labelling is according to the amino-acid identity in Mtb-DHDPR. Filled circles correspond to the respective closed conformations and open circles to the open conformations of the various DHDPR structures.

numbers show that subunit *E* may not be completely closed, although the surface contact area between the two domains calculated by the *PISA* server (Krissinel & Henrick, 2005) indicates that it is indeed closed. The interface area between the two domains of subunit *A* (open) is 657 Å^2, while for subunit *E* (closed) it is 748 Å^2, which is nearly the same value as can be calculated for subunit *A* from PDB entry 1p9l (751 Å^2). The difference in the swing angle may thus just be a consequence of even the closed conformation still allowing some slight relative domain movement. Also, a certain variety of structures exist for the open conformation, indicating that some degrees of freedom also exist in this conformation. The swing angle between the most and the least open conformation for the structures reported here occurs between subunits *C* and *D* of the monoclinic crystal form *C*. It equals 14.6°, which explains the rather high r.m.s. difference for this structure pair (Table 3).

In order to elucidate which amino-acid residues are the key residues that are responsible for the conformational changes, a torsion-angle analysis of the linker residues was carried out for all available DHDPR structures from *M. tuberculosis*, *E. coli* and *T. maritima* (Table 5, Fig. 6). For the structure of Tm-DHDPR the situation seems obvious. The only significant change in the main-chain (φ, ψ) torsion angles in the first linker region occurs for Ser99, which corresponds to Ala106 in Mtb-DHDPR and to Ser130 in Ec-DHDPR. The values of both angles change by approximately 30° when the open and closed conformers are compared with each other (Table 5). The situation appears to be similar for the second linker, where the most dramatic change occurs for Ser183 (Asp213 in Mtb-DHDPR and Ser239 in Ec-DHDPR), where the φ angle changes by approximately 25°. The same analysis has been carried out for Ec-DHDPR. Here, PDB entry 1arz (Scapin *et al.*, 1997) was used, which contains both open and closed conformers. In contrast to Tm-DHDPR, the changes in the main-chain torsion angles in Ec-DHDPR are spread out over a few residues, namely the stretches Asn129–Ser130 and Ser239–Met241, which correspond to the fragments Asn104–Ala106 and Asp213–Thr215 in Mtb-DHDPR. The situation appears to be more complicated for Mtb-DHDPR. The variation in the main-chain torsion angles is rather high, especially for the subunits from the two orthorhombic crystal forms. Some of the torsion-angle values are closer to the open conformation, while others are reminiscent of the closed

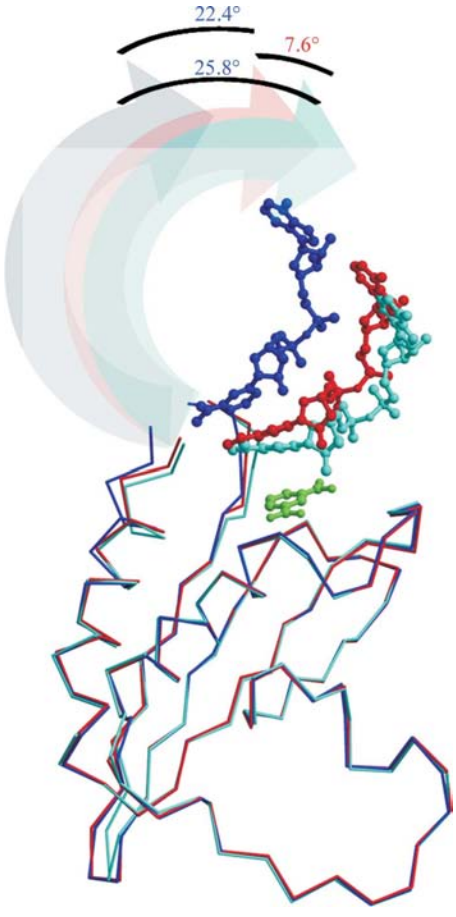

Figure 7
Illustration of the swing angle, which is defined as the angle that relates the open to the closed conformation of DHDPR. For clarity, only the tetramerization domain of DHDPR is shown. The molecules are labelled as follows. Chains *A* and *E* from the monoclinic crystal form *C* are shown in blue and red, respectively. Cyan represents subunit *A* of the fully closed ternary complex of DHDPR with NADH and the inhibitor 2,6-PDC (PDB entry 1p9l; Cirilli *et al.*, 2003). The NADH molecules are coloured according to the structure to which they belong, while the inhibitor 2,6-PDC from PDB entry 1p9l is shown in green.

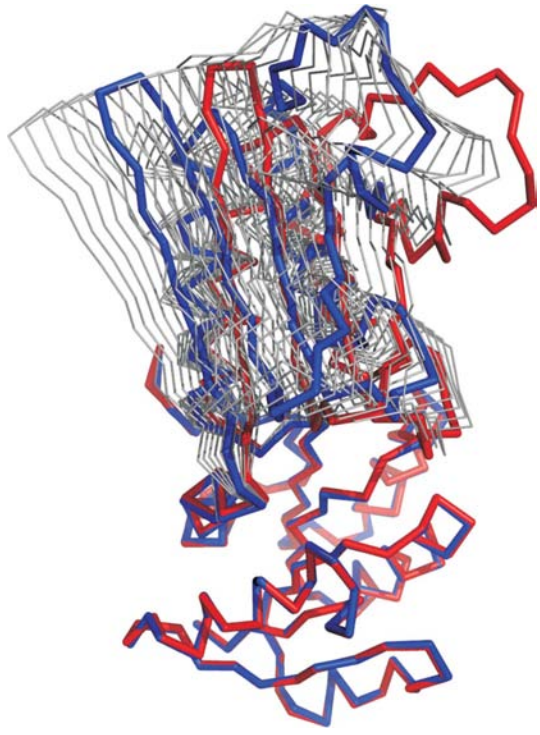

Figure 8
Superposition of the open (chain *A*, dark blue) and closed (chain *E*, red) conformers observed in crystal form *C* (PDB entry 1yl7) with the low-frequency normal modes calculated using the *ElNémo* server (Suhre & Sanejouand, 2004). 11 coordinate sets are shown (in grey) which were derived from the open conformation (in dark blue) of Mtb-DHDPR. The most closed of these 11 conformations fits well to the observed closed conformation of Mtb-DHDPR (in red). This figure was prepared with *PyMOL* (DeLano, 2002).

conformation. If, however, crystal forms *A* and *B* are excluded from the analysis, only the ψ angles of residues Ala106 and Asp213 in the first and second linker change by more than 10° between the two conformations. This may indicate that these two residues are of central importance for the movement of the domains, which is in accord with what has been observed for Ec-DHDPR and Tm-DHDPR. A visual impression of the changes in main-chain dihedral angles is given in the Ramachandran plot-like Fig. 6. This also shows that the clearest picture is obtained for Asn104, Ala106 and Asp213.

3.7. Normal-mode analysis

The results of the normal-mode analysis of Mtb-DHDPR are illustrated in Fig. 8. The mode depicted is the low-frequency normal mode No. 9, which was obtained from the observed open conformer (PDB entry 1yl7, chain *A*). The fit of the predicted most closed conformer and the observed closed conformer (PDB entry 1yl7, chain *E*) is very good, as evidenced by an r.m.s.d. value of 1.77 Å. When the flexible loop comprising residues Leu158–Asp178 was excluded from the calculation, the value was 0.67 Å. While in the tetramer this loop is involved in many intermolecular interactions and is rather rigid, as is the whole tetramerization domain, in the monomer it is solvent-exposed and the normal-mode program treats it as flexible. Consequently, in all calculated normal modes this loop exhibits very high mobility. However, for the interpretation of the domain the movement of this loop appears not to be important. When the normal-mode calculation is repeated based on the observed closed conformer (chain *E*), the low-frequency normal mode No. 11 yields the most open conformer, which is structurally very similar to the observed open conformer (chain *A*) as evidenced by r.m.s.d. values of 1.68 and 1.05 Å when including or excluding the loop Leu158–Asp178, respectively (not shown). It is also interesting to note that based on the normal-mode analysis an even more closed conformation than the observed closed conformation (not shown) and an even more open conformation than the observed open conformation (see Fig. 8) are predicted. This means that the crystallographically observed structures may not describe the extreme points of what the molecule is capable of in solution.

4. Conclusions

Three-dimensional structures of dihydrodipicolinate reductase from *M. tuberculosis* in its apo form and as a binary complex with the cofactor NADH have been determined and described from three different crystal forms. In solution, Mtb-DHDPR occurs as a tetramer as observed by size-exclusion chromatography and dynamic light-scattering experiments. In all three crystal forms the same homotetramer of Mtb-DHDPR occurs as the main building block. While in crystal forms *A* and *B* an Mtb-DHDPR dimer forms the asymmetric unit and the homotetramer is created *via* a crystallographic twofold axis, crystal form *C* harbours two complete tetramers in its asymmetric unit. In the latter crystal form all eight subunits in the asymmetric unit contain the cofactor NADH bound to the N-terminal nucleotide-binding domain. Analysis of the relative domain orientations in all independent Mtb-DHDPR subunits indicates that 11 of the 12 molecules occur in the open conformation of the enzyme, while the remaining molecule, subunit *E* in crystal form *C*, occurs in the closed conformation. This is a surprising observation since previous studies (Cirilli *et al.*, 2003; Scapin *et al.*, 1997; Joint Center for Structural Genomics, unpublished data) had indicated that the closed conformation of the enzyme occurs only after binding both cofactor and substrate or inhibitor. However, it cannot be excluded that the observed closed conformation of Mtb-DHDPR in complex with NADH as observed in subunit *E* of crystal form *C* is a crystallization artifact, since an open conformation of this subunit would not fit into the crystal packing. A detailed analysis of the different conformations observed for DHDPRs from *M. tuberculosis*, *E. coli* and *T. maritima* revealed that the three residues Asn104, Ala106 and Asp213 of Mtb-DHDPR (and the corresponding residues in the other DHDPRs), which are part of the two observed hinge regions, play a crucial role in the domain rearrangements of DHDPR which occur along the reaction coordinate. The large conformational changes observed in Mtb-DHDPR can be rationalized as a motion along one of the low-frequency normal modes of the protein.

We would like to thank Dr L. Jeanne Perry (UCLA) for providing genomic Mtb H37Rv DNA, Linda Schuldt (EMBL Hamburg) for the preparation of Fig. 1, Dr Santosh Panjikar (EMBL Hamburg) for his help and input in solving the structure of crystal form *C* of Mtb-DHDPR, the TB consortium (http://www.doe-mbi.ucla.edu/TB) for postdoctoral exchange grants to GK and the X-Mtb consortium (http://www.xmtb.org) for funding through BMBF/PTJ grant No. BIO/0312992A.

References

Cirilli, M., Zheng, R., Scapin, G. & Blanchard, J. S. (2003). *Biochemistry*, **42**, 10644–10650.
Cohen, G. E. (1997). *J. Appl. Cryst.* **30**, 1160–1161.
Cole, S. T. *et al.* (1998). *Nature (London)*, **393**, 515–516.
Collaborative Computational Project, Number 4 (1994). *Acta Cryst.* D**50**, 760–763.
Cox, R. J. (1996). *Nat. Prod. Rep.* **13**, 29–43.
DeLano, W. L. (2002). *PyMOL Molecular Viewer.* DeLano Scientific LLC, Palo Alto, California, USA. http://www.pymol.org.
Grandoni, J. A., Marta, P. T. & Schloss, J. V. (1998). *J. Antimicrob. Chemother.* **42**, 475–482.
Hayward, S. & Berendsen, H. J. C. (1998). *Proteins*, **30**, 144–154.
Hutton, C. A., Southwood, T. J. & Turner, J. J. (2003). *Mini Rev. Med. Chem.* **3**, 115–127.
Jones, T. A., Zou, J.-Y., Cowan, S. W. & Kjeldgaard, M. (1991). *Acta Cryst.* A**47**, 110–119.
Kabsch, W. (1976). *Acta Cryst.* A**32**, 922–923.
Kefala, G., Janowski, R., Panjikar, S., Mueller-Dieckmann, C. & Weiss, M. S. (2005). *Acta Cryst.* F**61**, 718–721.
Krissinel, E. & Henrick, K. (2004). *Acta Cryst.* D**60**, 2256–2268.
Krissinel, E. & Henrick, K. (2005). *CompLife 2005*, edited by M. R. Berthold, R. Glen, K. Diederichs, O. Kohlbacher & I. Fischer, pp. 163–174. Berlin, Heidelberg: Springer-Verlag.

Kraulis, P. J. (1991). *J. Appl. Cryst.* **24**, 946–950.
Laskowski, R. A., MacArthur, M. W., Moss, D. S. & Thornton, J. M. (1993). *J. Appl. Cryst.* **26**, 283–291.
Merritt, E. A. & Bacon, D. J. (1997). *Methods Enzymol.* **277**, 505–524.
Murshudov, G. N., Vagin, A. A. & Dodson, E. J. (1997). *Acta Cryst.* D**53**, 240–255.
Paiva, A. M., Vanderwall, D. E., Blanchard, J. S., Kozarich, J. W., Williamson, J. M. & Kelly, T. M. (2001). *Biochim. Biophys. Acta*, **1545**, 67–77.
Pavelka, M. S., Weisbrod, T. R. & Jacobs, W. R. Jr (1997). *J. Bacteriol.* **179**, 2777–2782.
Reddy, S. G., Sacchettini, J. C. & Blanchard, J. S. (1995). *Biochemistry*, **34**, 3492–3501.
Reddy, S. G., Scapin, G. & Blanchard, J. S. (1996). *Biochemistry*, **35**, 13294–13302.
Rossmann, M. G., Liljas, A., Brändén, C.-I. & Banaszak, L. J. (1975). *The Enzymes*, 3rd ed., edited by P. D. Boyer, Vol. 11A, pp. 61–102. New York: Academic Press.
Sassetti, C. M., Boyd, D. H. & Rubin, E. J. (2003). *Mol. Microbiol.* **48**, 77–84.
Scapin, G., Blanchard, J. S. & Sacchettini, J. C. (1995). *Biochemistry*, **34**, 3502–3512.
Scapin, G., Reddy, S. G., Zheng, R. & Blanchard, J. S. (1997). *Biochemistry*, **36**, 15081–15088.
Schneider, T. R. (2002). *Acta Cryst.* D**58**, 195–208.
Suhre, K. & Sanejouand, Y. H. (2004). *Nucleic Acids Res.* **32**, W610–W614.
Vagin, A. & Teplyakov, A. (1997). *J. Appl. Cryst.* **30**, 1022–1025.
Wang, F., Blanchard, J. S. & Tang, X. J. (1997). *Biochemistry*, **36**, 3755–3759.
Winn, M. D., Isupov, M. N. & Murshudov, G. N. (2001). *Acta Cryst.* D**57**, 122–133.